# Middle Cell Development for Wafer-Bonded III-V//Si Tandem Solar Cells

Patrick Schygulla [ID], Friedemann D. Heinz, Frank Dimroth [ID], and David Lackner

*Abstract*—This article focuses on the material properties of two III-V semiconductors, AlGaAs and GaInAsP, and their usage as middle cell absorber materials in a wafer-bonded III-V//Si triple-junction solar cell. To this end single-junction solar cells were grown epitaxially lattice matched on GaAs wafers using metalorganic vapor phase epitaxy. By optimizing the growth temperature and the V/III ratio we could increase the open-circuit voltage at a target absorber band gap of 1.50 eV by up to 100 mV. In the future these results will be implemented into two-terminal III-V//Si triple-junction solar cells to increase the conversion efficiency beyond 35% under the AM1.5g solar spectrum.

*Index Terms*—AlGaAs, GaInAsP, III-V//Si, metalorganic vapor phase epitaxy (MOVPE), multijunction solar cells.

## I. INTRODUCTION

**M**ULTIJUNCTION solar cell devices have demonstrated efficiencies above 38% [1] under the AM1.5g spectrum, due to an efficient utilization of the solar spectrum. Single junction devices are limited to a maximum efficiency of 33% by radiative recombination [2]. In the case of the indirect semiconductor silicon, which is ultimately limited by Auger recombination, the theoretically calculated conversion efficiency is between 29.5% and 29.6% when light trapping is considered [3], [4]. Multijunction solar cells, though, are not yet cost competitive for flat panel applications with conventional single-junction Si solar cells due to high substrate, precursor, facility, and production costs. Already demonstrated growth rates above 120 mm/h [5], [6] as well as substrate removal and reuse [7] will help to reduce manufacturing costs in the future, especially when combined with a low cost silicon bottom solar cell which serves simultaneously as a substrate. Such III-V/Si multijunction solar cells can be realized either by metamorphic growth or bond. Such III-V//Si multijunction solar cells were demonstrated to reach efficiencies of 35.9% [8] in the case of a four-terminal mechanical stack and exceeding 34% [9], [10] in the case of a monolithically integrated two-terminal configuration using a direct wafer bond.
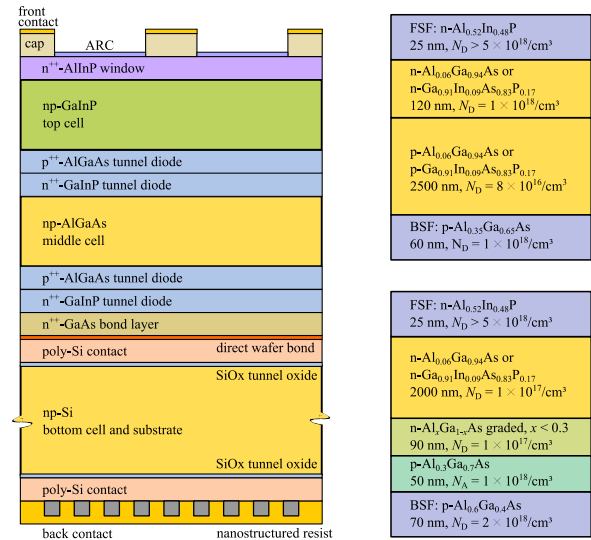
Fig. 1. Left: III-V//Si triple-junction solar cell layer stack with an efficiency of 34.1% under AM1.5g. The currently used middle cell consists of a mostly p-type AlGaAs absorber in a homojunction design. Right: Structures of the homo-junction (top) and rear-heterojunction (bottom) component cells that are examined in this article.

A schematic of the layer stack of the latter device is shown in Fig. 1(left). Compared to the top $Ga_{0.51}In_{0.49}P$ (GaInP) subcell the middle cell with a p-$Al_{0.06}Ga_{0.94}As$ (AlGaAs) absorber; however, has still a higher loss to the radiative limit on substrate of 123 mV. Therefore, in this article, we show how the performance of the second junction can be improved. In order to exploit the full potential of this cell architecture, absorber materials at the optimum band gap with long minority carrier lifetimes are essential. There are indications that n-AlGaAs exhibits superior material quality compared to the p-type material when used in a rear heterojunction cell design [11]. Thus, we studied n-AlGaAs as a potential replacement for the currently used p-type middle cell absorber. Another interesting alternative is GaInAsP lattice matched to GaAs. It was demonstrated as solar cell absorber material[1] in the band gap range between 1.6 and 1.7 eV [12], [13]. The optimum band gap combination in the radiative limit for a triple-junction cell with Si at the bottom would be 2.01 and 1.50 eV for the top and middle cell, respectively. Although we consider a GaInP top cell with a band gap of 1.90 eV, the middle cell target band gap remains at 1.50 eV albeit with a slightly reduced efficiency potential by 3% as device simulations with the software EtaOpt [14] have shown. Hence, 1.50 eV is the design band gap of the materials investigated in this article.

We have already reported on a detailed material comparison between the quaternary n-$Ga_{0.91}In_{0.09}As_{0.83}P_{0.17}$ (GaInAsP), the ternary n-AlGaAs, and the reference material p-AlGaAs as absorber layer in a III-V//Si triple-junction solar cell [15]. In this enhanced article, we extend the study to investigating the diffusion length achieved in these materials and the influence of different minority barrier layers that could be used as front- or back-surface fields (BSFs) in the subcell. In addition, we report on optical simulations concerning the required absorber thickness as a function of band gap and how this relates to the measured diffusion length.

## II. Materials and Methods

### A. Epitaxial Growth

Test samples were grown in an AIXTRON 2800G4-TM reactor using metalorganic vapor phase epitaxy (MOVPE) on 4" GaAs wafers with a 6° miscut of the (100) surface toward (111)B. The precursors used for growing the GaAs, AlGaAs, and GaInAsP layers were trimethylgallium (TMGa), arsine (AsH$_3$), trimethylaluminium (TMAl), trimethylindium (TMIn), and phosphine (PH$_3$). The growth conditions were varied in order to identify the set of growth parameters that results in the highest material quality, respectively. The growth temperature was investigated between 580 to 640 °C. The nominal V/III-ratio was varied between 10 and 65 while the growth rate was kept constant at 1.3 nm/s for GaInAsP and 1.6 nm/s for AlGaAs. Double-heterostructures (DH) consisting of the material under investigation with a thickness of 500 nm surrounded by two 50 nm thick $Ga_{0.51}In_{0.49}P$ barrier layers (for GaInAsP) and 100 nm thick $Al_{0.7}Ga_{0.3}As$ barrier layer (for AlGaAs) were grown. These test samples served for determining the composition as a function of growth conditions and for measurements of the minority carrier lifetimes. The materials were then incorporated as absorber layers in single-junction solar cell devices. The p-AlGaAs absorber was included in an n-on-p homojunction solar cell design as is the case for the middle cell in the current III-V//Si triple-junction device. The n-type absorber materials, though, were integrated as n-on-p rear-heterojunction solar cells [16]. The AlGaAs and GaInAsP absorber layers were doped to the same level in order to allow for a direct comparison of the material quality. The structures of the investigated solar cells are summarized in Fig. 1 (right). For the growth parameter study rudimentary cell processing of 6 cm² cells was employed. After optimization 4 cm² solar cells were fully processed. No anti-reflection coating (ARC) was deposited on the cells.

### B. Material and Solar Cell Characterisation

The composition of the $Ga_{1-x}In_xAs_{1-y}P_y$ layers was determined by a combination of the out-of-plane lattice constant from X-ray diffraction and the band gap from spectral photoluminescence (PL). The composition of the $Al_xGa_{1-x}As$ layers was calculated from the PL-determined band gap with data from [17]. The spectral PL measurements were conducted at room temperature using a frequency doubled diode-pumped solid-state laser emitting at 532 nm. The photon wavelengths of the PL signal recorded by a charge-coupled device (CCD)

camera were first calibrated using Neon spectral lines. The absorption threshold, which was interpreted as the band gap was then obtained by the position of the maximum in the first derivative of the calibrated PL signal [18]. The effective minority carrier lifetime was measured by exponential fits to the PL signal transient decay after 10 ns of excitation with a 515 nm digitally modulated laser at 1 mW resulting in an injection level below $10^{11}$/cm³. Such a low excess carrier density allows to probe the minimum lifetime regime in which the effective lifetime is dominated by Shockley-Read-Hall recombination and thus offers a direct material quality comparison. Time resolved PL (TRPL) is recorded at room temperature using the time correlated single photon counting technique and a hybrid photodetector. Exploiting the linear dependence of PL signal and $\Delta n$ at low injection conditions the minority carrier lifetime $\tau$ is obtained from an exponential fit to the PL decay after the laser pulse. The lifetime $\tau$ is related to the implied open-circuit voltage

$$V_{\mathrm{oc,\,i}} = \frac{k_\mathrm{B}T}{q}\ln\left(\frac{(N_{\mathrm{A/D}} + \Delta n)\,\Delta n}{n_\mathrm{i}^2}\right) \tag{1}$$

via the excess carrier density $\Delta n = G\tau$ assuming an ideality factor of 1 [19]. Here, $k_\mathrm{B}$ denotes Boltzmann's constant, $T$ the temperature, $q$ the elementary charge, $N_{\mathrm{A/D}}$ the doping density for p-type or n-type doping, respectively, $n_\mathrm{i}$ the intrinsic carrier density, and $G$ the charge carrier generation rate. Typical values for the excess carrier densities of the presented devices under AM1.5g are on the order of $10^{12}$ to $10^{13}$/cm³.

The carrier diffusion length

$$\mathrm{L} = \sqrt{D\tau} \tag{2}$$

with diffusion coefficient $D$ is a useful parameter for assessing the current collection efficiency by comparing it to the absorber layer thickness. However, due to the square-root dependence on minority carrier lifetime it is less sensitive to the material quality compared to the lifetime itself. The carrier diffusion length was determined for n- and p-$Al_{0.06}Ga_{0.94}As$ and n-GaInAsP DHs using cathodoluminescence [20]. For each sample three different pieces were prepared and measured independently at three different spots in order to calculate the average and the standard deviation. Three different barrier materials, $Ga_{0.51}In_{0.49}P$, $Al_{0.3}Ga_{0.7}As$, and $Al_{0.8}Ga_{0.2}As$, were investigated in order to study the impact of the crystallographic interface on the diffusion length. The doping level of the barriers, $2 \times 10^{18}$/cm³, was significantly higher than the doping level of the bulk material, $3 \times 10^{17}$/cm³, in order to provide an efficient minority carrier barrier as in the solar cell device.

The open-circuit voltage of the single-junction solar cells was determined using the suns-$V_\mathrm{oc}$ method [21]. Along with the band gap $E_\mathrm{g}$ for the absorber material, the maximum achievable open-circuit voltage

$$V_{\mathrm{oc,rad}}\,(E_\mathrm{g}) = \frac{E_\mathrm{g}}{q} - \frac{k_\mathrm{B}T}{q}\ln\left(\frac{2\pi\left(1 + n_\mathrm{sub}^2\right)qE_\mathrm{g}k_\mathrm{B}T}{h^3c^2j_\mathrm{ph}}\right) \tag{3}$$

could then be calculated [22] in the radiative limit on a substrate for a photon current $j_\mathrm{ph}$ given a solar spectrum as AM1.5g in our case. The refractive index needs to be taken at the wavelength of
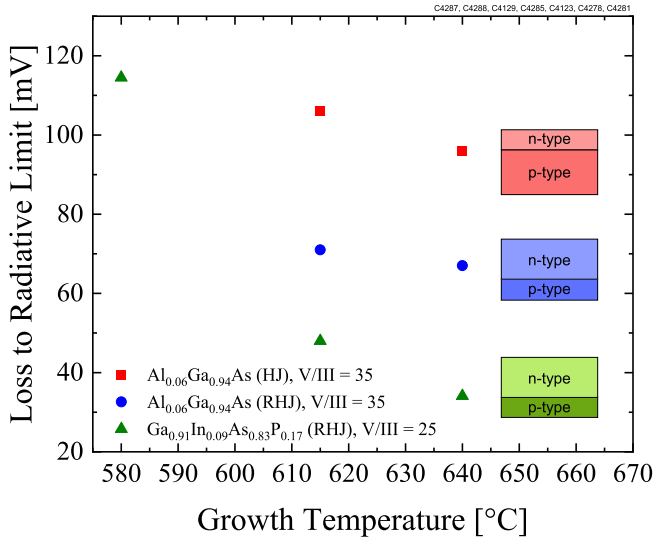
Fig. 2. Difference between the maximum voltage in the radiative limit on substrate as calculated from (3) and the measured open-circuit voltage as a function of the growth temperature at constant V/III-ratio. The solar cell samples have a mostly p-type $Al_{0.06}Ga_{0.94}As$ absorber in homojunction design (HJ, red), an $n-Al_{0.06}Ga_{0.94}As$ absorber in rear-heterojunction design (RHJ, blue), or an $n-Ga_{0.91}In_{0.09}As_{0.83}P_{0.17}$ absorber in RHJ design (green). The thicknesses amounted to 1.6 μm for the RHJ and 2.5 μm for the HJ solar cells, whereas the other structural parameters are identical to Fig. 1.
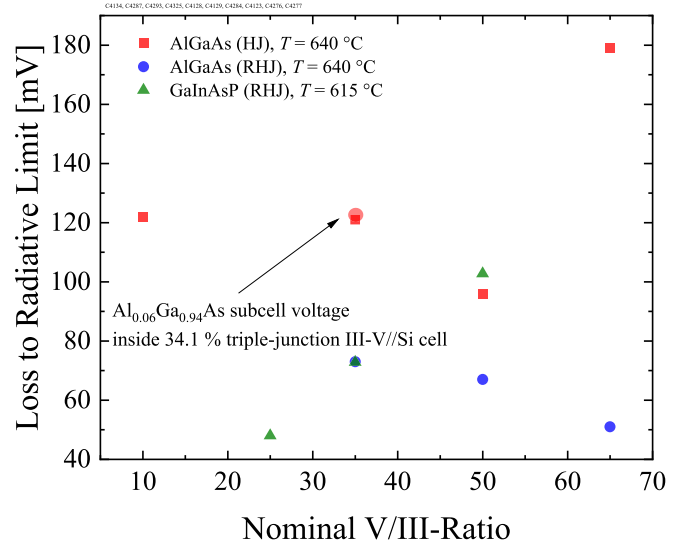


Fig. 3. Difference between the maximum voltage in the radiative limit on substrate as calculated from (3) and the measured open-circuit voltage as a function of the nominal V/III-ratio at constant growth temperature. The solar cell samples have a mostly p-type $Al_{0.07}Ga_{0.93}As$ absorber in homojunction design (HJ, red), an $n-Al_{0.07}Ga_{0.93}As$ absorber in rear-heterojunction design (RHJ, blue), or an $n-Ga_{0.91}In_{0.09}As_{0.83}P_{0.17}$ absorber in RHJ design (green) absorber layer. The thicknesses amounted to 1.6 μm for the RHJ and 2.5 μm for the HJ solar cells.

the luminescent photons that are reemitted from the band edge, that is $n_{sub} = n_{sub}(E_g)$. Subtracting the measured $V_{oc}$ from the ideal case yields a figure of merit, the loss to the radiative limit on substrate, which is independent of absorber band gap. It thus provides a fair comparison between absorber materials with different band gaps. The external quantum efficiency and the reflection were measured in a LOANA setup [23].

The absorption in every subcell was calculated for the case of an $Al_xGa_{1-x}As$ middle cell using a transfer matrix modeling approach [24] of the layer stack shown in Fig. 1. The optical parameters required for this calculation were generated for each composition using a parameter morphing algorithm between GaAs and $Al_{0.3}Ga_{0.7}As$ [25]. Parasitic absorption in barrier, bond, and tunnelling diode layers were taken into account. Knowing the absorption, the current generation can then be tuned in the model to achieve current match between all subcells by adjusting the absorber thicknesses. The required thickness for the middle cell as a function of absorber band gap is then compared to the minority carrier diffusion length.

Band diagram simulations were performed with the software nextnano [26] in order to calculate the expected minority carrier barrier height for different passivating layers.

## III. RESULTS AND DISCUSSION

### A. Optimization of Growth Conditions

Higher growth temperatures result in higher voltages or correspondingly lower losses to the radiative limit for all three studied material systems. Increasing the growth temperature from 615 to 640 °C resulted in a voltage gain of 10–20 mV as can be seen in Fig. 2.

A similar strong impact on the cell performance is obtained by varying the V/III-ratio which is shown in Fig. 3. For p-AlGaAs there is an optimum V/III-ratio at around 50. For n-AlGaAs, however, yet higher V/III-ratios are beneficial. For n-AlGaAs the loss to the radiative limit decreases with increasing V/III-ratio between 35 and 65, suggesting that there are two different dominant defects with opposite dependencies on the V/III-ratio. Suppression of oxygen incorporation could be the explanation for the increased voltages at higher V/III-ratios in n-AlGaAs. If the V/III-ratio is increased further, an increasing formation probability for $As_{Ga}$-antisite defects is expected [5]. This would cause a voltage decrease as it was observed for p-AlGaAs. The loss to the radiative limit of the current p-AlGaAs middle cell (red circle in Fig. 3) is similar to the corresponding single-junction. For n-GaInAsP the loss to the radiative limit increases between a nominal V/III-ratio of 25 and 50 by 50 meV. As opposed to AlGaAs GaInAsP is less affected by the parasitic incorporation of oxygen so one possible explanation may be the more dominant influence of the $As_{Ga}$ antisite defect. For GaAs solar cells improved material quality is achieved at lower V/III ratios as reported in the literature [27].

### B. Material Comparison

After optimizing each material system individually, a direct comparison of the respective best solar cells can be conducted. In Fig. 4 the internal quantum efficiency $IQE = EQE/(1-R)$ of an n-AlGaAs cell is compared to an n-GaInAsP cell. Here, $EQE$ refers to the external quantum efficiency and $R$ to the reflection from the cell surface. The $IQE$ curves were corrected in height according to the measured short-circuit currents from the corresponding $IV$-measurements. One can see that throughout the
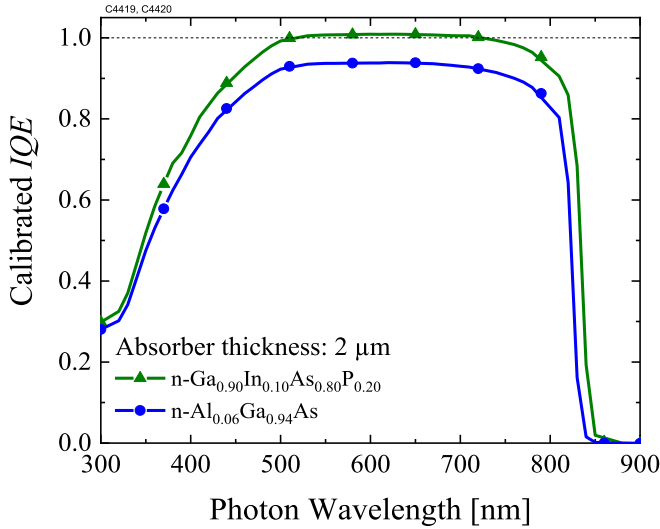
Fig. 4. Internal quantum efficiency, calibrated with respect to the short-circuit current, of an n-$Al_{0.06}Ga_{0.94}As$ (blue) and an n-$Ga_{0.90}In_{0.10}As_{0.80}P_{0.20}$ (green) rear-heterojunction solar cell with 2 μm absorber layer thickness. The cells do not have an anti-reflection coating. The maximum IQE is 1.009. This apparently unphysical value is still within the uncertainty of the measurement and the calibration procedure. which amounts to around 2–3%.



Fig. 5. Current-voltage characteristics of an $Al_{0.06}Ga_{0.94}As$ (blue) and a $Ga_{0.90}In_{0.10}As_{0.80}P_{0.20}$ (green) rear-heterojunction solar cell with the same absorber layer thickness of 2 μm.

entire wavelength range n-GaInAsP exhibits a higher quantum efficiency compared to n-AlGaAs. The largest difference occurs at intermediate wavelengths between 550 and 800 nm in the constant plateau region. The absorber thickness is 2 μm for both cells. Hence, the reduced *IQE* cannot be explained by a lower absorption in n-AlGaAs. Rather, poor charge carrier extraction because of an insufficient minority carrier diffusion length in this material is the reason. This is not completely unexpected as AlGaAs tends to show a number of known defects: The reason for the lower material quality in AlGaAs might be related to the presence of deep recombination centres associated with oxygen impurities. Due to its high affinity to aluminium, oxygen atoms can be more easily incorporated into the AlGaAs than into the GaInAsP crystal lattice [28].

The current-voltage characteristics are presented in Fig. 5. A gain in short-circuit current density $j_{sc}$ of 1.8 mA/cm² can be achieved if n-$Ga_{0.90}In_{0.10}As_{0.80}P_{0.20}$ is used instead of n-$Al_{0.06}Ga_{0.94}As$ for the absorber material at constant layer thickness. This can partly be understood by the band gap of the latter, which is 10 meV higher resulting in less absorption of the solar spectrum. By integrating this part of the solar spectrum one finds that this effect can explain 0.6 mA/cm² at maximum. Thus, the remaining difference of 1.2 mA/cm² is caused by the higher quantum efficiency in n-GaInAsP compared to n-AlGaAs shown in Fig. 4. In the given target band gap range of around 1.50 eV n-GaInAsP can be grown with excellent material quality using MOVPE yielding lower losses to the radiative limit than n-AlGaAs. The solar cell made of an n-GaInAsP absorber achieves a higher open-circuit voltage than the n-AlGaAs based cell despite its slightly lower absorber band gap. To put this comparison in an absolute context a solar cell with the given band gap and thickness would achieve a $V_{oc}$ of 1.152 V in the radiative limit and a $j_{sc}$ of 29.3 mA/cm² from integration of the solar spectrum. It has to be noted, though, that around a third
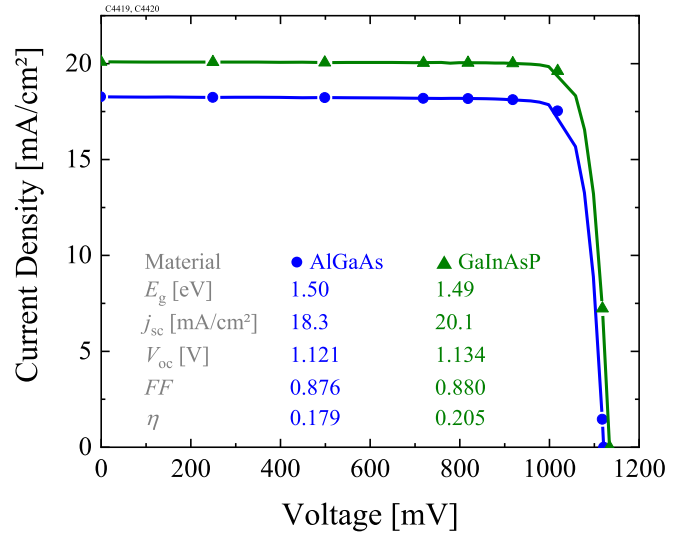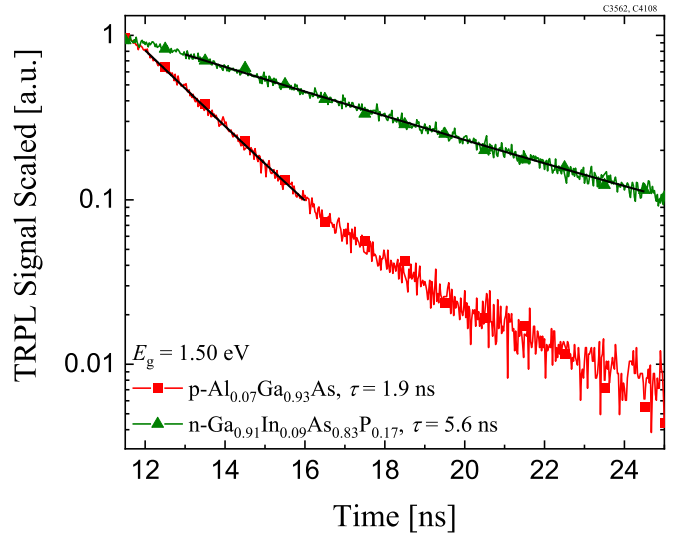


Fig. 6. Comparison of the signal decay transients from TRPL measurements of p-$Al_{0.07}Ga_{0.93}As$ (red, squares) and n-$Ga_{0.91}In_{0.09}As_{0.83}P_{0.17}$ (green, triangles) at the same band gap of 1.50 eV. In black the monoexponential fits that were used to extract the minority carrier lifetimes are shown. The nonmonoexponential tail at low signal intensities is caused by parasitic luminescence from within the setup and not sample related.

of the photocurrent is lost to the cell due to reflection (no ARC used) and parasitic absorption in the window layer.

The solar cell results are consistent with measurements of the minority carrier lifetime in test structures. Higher lifetimes result in higher excess carrier densities and consequently in higher voltages according to (1). The results, 1.9 ns for p-AlGaAs and 5.6 ns for n-GaInAsP, are in agreement with literature values for p-AlGaAs, 2–4 ns [29], or n-GaAs, 6.2 ns [30], respectively, for similar doping levels and very low injection levels. In Fig. 6 a direct comparison of the normalized TRPL transients is provided. Standard growth conditions were applied to all DHs to ensure the comparability of results while the above discussed improvements in growth temperature and V/III-ratio

TABLE I
MINORITY CARRIER DIFFUSION LENGTHS OF SAMPLES WITH
DIFFERENT BARRIER LAYERS

| Material | Bottom Barrier | Top Barrier | Diff. Length [μm] |
|---|---|---|---|
| n-Ga$_{0.90}$In$_{0.10}$As$_{0.85}$P$_{0.15}$ | Ga$_{0.51}$In$_{0.49}$P | Ga$_{0.51}$In$_{0.49}$P | 2.5 ± 0.2 |
| n-Al$_{0.06}$Ga$_{0.94}$As | Ga$_{0.51}$In$_{0.49}$P | Ga$_{0.51}$In$_{0.49}$P | 1.8 ± 0.1 |
| n-Al$_{0.06}$Ga$_{0.94}$As | Ga$_{0.51}$In$_{0.49}$P | Al$_{0.3}$Ga$_{0.7}$As | 2.2 ± 0.1 |
| n-Al$_{0.06}$Ga$_{0.94}$As | Ga$_{0.51}$In$_{0.49}$P | Al$_{0.8}$Ga$_{0.2}$As | 1.6 ± 0.1 |
| p-Al$_{0.06}$Ga$_{0.94}$As | Ga$_{0.51}$In$_{0.49}$P | Al$_{0.3}$Ga$_{0.7}$As | 2.0 ± 0.1 |
| p-Al$_{0.06}$Ga$_{0.94}$As | Al$_{0.8}$Ga$_{0.3}$As | Al$_{0.8}$Ga$_{0.3}$As | 2.5 ± 0.1 |

Thickness was kept constant at 500 nm and the doping level was similar (between 2.46 to $3.12 \times 10^{17}$/cm³) in all samples.
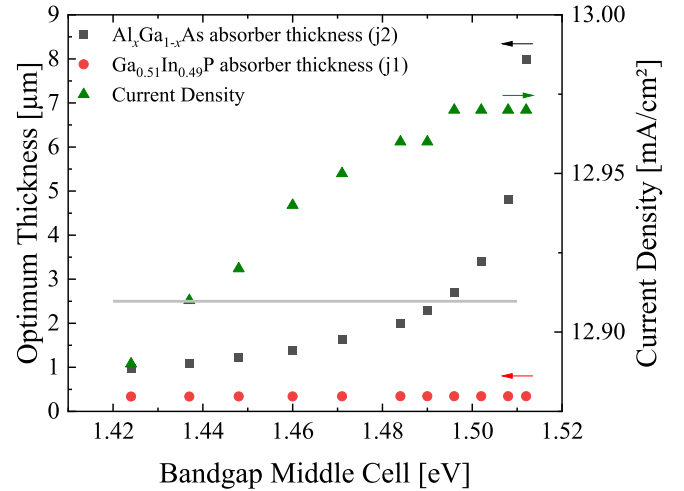


Fig. 7. Required thickness of middle cell absorber layer as a function of the band gap to achieve current matching conditions in a III-V//Si triple-junction solar cell. The grey line indicates a reference value for the diffusion length in p-AlGaAs as measured by cathodoluminescence.

were implemented for the growth of solar cells. This may lead to different absolute values for the effective diffusion length and lifetime in test layers and solar cell absorbers.

The diffusion length measurements also reveal higher performance of n-GaInAsP compared to both n- and p-AlGaAs. At the same doping level of $3 \times 10^{17}$/cm³, the same thickness of 500 nm and using Ga$_{0.51}$In$_{0.49}$P as both top and bottom barrier the holes in n-GaInAsP have a diffusion length of 2.5(2) μm while in n-Al$_{0.06}$Ga$_{0.94}$As they have a diffusion length of 1.8(1) μm, cf. Table I. It should be noted that although the barrier material is the same in both cases, the interface may still show differences caused by a different MOVPE switching sequence.

### C. Choice of Barriers

In the current design of the III-V//Si triple-junction solar cell a p-Al$_{0.3}$Ga$_{0.7}$As BSF is used as a rear-side minority carrier barrier. In order to improve the subcell voltage and the carrier collection efficiency, the diffusion lengths of the carriers in the same n- and p-Al$_{0.06}$Ga$_{0.94}$As bulk material with different barrier materials are compared to each other in Table I. In the n-type material replacing the Al$_{0.3}$Ga$_{0.7}$As barrier on one side with Ga$_{0.51}$In$_{0.49}$P reduces the diffusion length from 2.2 to 1.8 μm. Increasing the aluminium content of the barrier to 0.8 further reduces the diffusion length to 1.6 μm. Comparing p- and n-type Al$_{0.06}$Ga$_{0.94}$As with the same barriers one finds that the minority diffusion length in p-type material is slightly lower than in n-type but still within the standard deviation of the measurements.

Since not only the minority carrier lifetime but also the minority carrier mobility changes from p- to n-type material this method cannot resolve which material has the higher bulk material quality but only whether the obtained diffusion lengths are compatible with the desired absorber thickness within the solar cells. For p-Al$_{0.06}$Ga$_{0.94}$As the high-aluminium Al$_{0.8}$Ga$_{0.2}$As barriers yield the highest observed diffusion length of 2.5 μm. Band simulations show that the band alignment produces a larger minority carrier barrier of 430 meV height in the case of n-Ga$_{0.51}$In$_{0.49}$P/n-Al$_{0.06}$Ga$_{0.94}$As compared to one of 320 meV in the case of n-Al$_{0.3}$Ga$_{0.7}$As/n-Al$_{0.06}$Ga$_{0.94}$As. As the diffusion length is smaller for the n-Ga$_{0.51}$In$_{0.49}$P barrier despite of the higher barrier and despite of the occurrence of

nonradiative recombination centres, so called DX-centres, in n-Al$_{0.3}$Ga$_{0.7}$As:Si [31] this is an indication of a nonideal interface created during epitaxial growth at the arsenide-to-phosphide change. Although increasing the aluminium content of the barrier beyond 0.4 reduces the detrimental effect of the DX-centres because of its energetic position inside the band gap [32] we observed an even lower diffusion length for an n-Al$_{0.8}$Ga$_{0.2}$As:Si barrier. This could mean that the reduced lifetime in Al$_{0.8}$Ga$_{0.2}$As due to high oxygen impurity densities overrides the benefit of the higher barrier and thus decreased penetration of the wave function. As for the barrier on the p-side an option for the future to improve the promising p-Al$_{0.8}$Ga$_{0.2}$As barrier material further might be the inclusion of a thin Al$_{0.14}$Ga$_{0.86}$As interlayer between active layer and barrier as suggested by [33].

### D. Absorber Thickness

In order to maximize the power output of a III-V//Si triple-junction cell under the AM1.5g spectrum, the current contributions from the three subcells of the multijunction device must be matched. For a given top cell band gap the optimum thickness of the middle cell absorber layer is a function of the band gap of the material. In principle an increased band gap leads to a higher open-circuit voltage and thus efficiency potential until the short-circuit current is limited by a fully absorbing subcell. In reality the absorption thickness and thus the band gap is limited by the diffusion length. For every aluminium concentration $x$, corresponding to a certain (direct) band gap $E_{g,AlGaAs}(x) = (1.2475\,x + 1.422)$ eV [34] the required thickness for achieving current matching is plotted in Fig. 7. The maximum obtainable current density at current match slightly increases with increasing band gap due to reduced parasitic absorption and thus improved distribution of the available solar resource among the three subcells. Assuming a shading factor of 1.6% caused by the metal front contacts the current density for the employed structure converges to around 12.97 mA/cm²
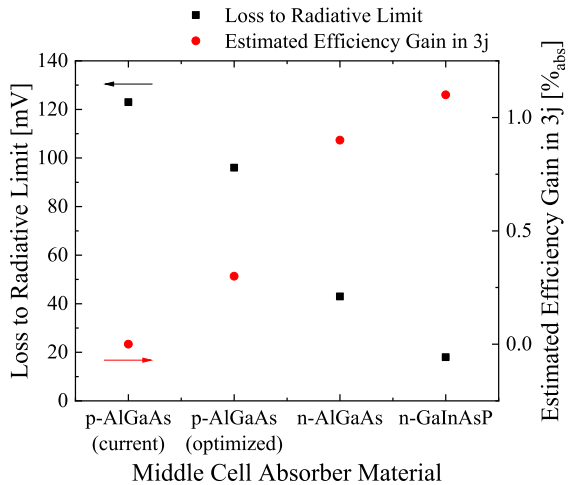
Fig. 8. Loss to the radiative limit on substrate for different materials having a band gap of around 1.5 eV (left axis). If used as middle cell absorber in a triple-junction III-V//Si solar cell the projected conversion efficiency gain is estimated (right axis). The mostly p-type absorbers are employed in a homojunction and the n-type absorbers are employed in a rear-heterojunction architecture. For the efficiency projection the current density and the filling factor of the triple-junction solar cell were assumed constant.

at absorber thicknesses exceeding 2 μm. This value is strongly influenced by the performance of the Si bottom cell and the quality of the rear-side grating. There is only a limited amount of energy and thus photon density available in the spectrum between the GaInP top cell absorber band gap of 1.89 eV, and the middle cell absorber band gap $E_{g,AlGaAs}(x)$ as well as between the latter and the silicon cell band gap of 1.12 eV. Therefore, the required thickness of the middle cell absorber layer diverges to infinity at a band gap of 1.528 eV. Increasing the band gap even further would result in a current limitation of the second junction unless the first junction is thinned accordingly, thus reducing the overall achieved current density. This sets one upper fundamental limit to the middle cell band gap, and consequently, subcell voltage. Another more practical limit is defined by the diffusion length of the charge carriers inside the absorber layer material. As shown in the last section the diffusion length depends strongly on the types of barriers used. A typical reference value of 2.5 μm is marked in Fig. 7 and compared to the required absorber layer thickness. In this case current matched triple-junctions with a middle cell band gap exceeding 1.49 eV would already exhibit a drop in quantum efficiency as is shown for the 2 μm thick single-junction n-Al$_{0.06}$Ga$_{0.94}$As cell in Fig. 4. The calculation of the required thickness at a given band gap holds to a good approximation also for GaInAsP since the thickness is mainly determined by the position of the absorption threshold and not the exact spectral dependence of the *n* and *k* data. Thanks to the superior material quality and thus higher diffusion length in n-GaInAsP at the same doping level, the thickness limit is lifted allowing for higher band gaps and as a consequence yet higher subcell voltages. It should be noted that the values for the diffusion length presented in Table I were obtained on 500 nm thick samples which experience a stronger impact of surface recombination. Hence, the grey line in Fig. 7 at 2.5 μm defines a worst case estimation.

## IV. CONCLUSION

MOVPE grown 1.5 eV solar cells consisting of n-GaInAsP and p- and n-AlGaAs absorber layers lattice matched on GaAs wafers were compared. Devices having a predominantly n-type absorber showed a loss to the radiative limit on substrate of minimum 43 mV at $j_{sc} = 18.3$ mA/cm² for n-AlGaAs and of 18 mV at $j_{sc} = 20.1$ mA/cm² for n-GaInAsP as summarized in Fig. 8. Both materials are sensitive to the V/III-ratios, but with an opposite dependence in the investigated range. From the investigated barriers Al$_{0.3}$Ga$_{0.7}$As seems to be the most promising option for n-type and Al$_{0.8}$Ga$_{0.2}$As for p-type Al$_{0.06}$Ga$_{0.94}$As. By replacing the current p-AlGaAs middle cell in the 34.1% GaInP/AlGaAs//Si two-terminal record device with the optimized n-GaInAsP subcell, a voltage increase of around 100 mV can be expected. This would result in an estimated efficiency of above 35% under the AM1.5g spectrum.

## REFERENCES

[1] M. Green *et al.*, "Solar cell efficiency tables (version 57)," *Prog. Photovolt.: Res. Appl.*, vol. 29, no. 1, pp. 3–15, 2021.
[2] W. Shockley and H. J. Queisser, "Detailed balance limit of efficiency of *p-n* junction solar cells," *J. Appl. Phys.*, vol. 32, no. 3, pp. 510–519, 1961.
[3] A. Richter, M. Hermle, and S. W. Glunz, "Reassessment of the limiting efficiency for crystalline silicon solar cells," *IEEE J. Photovolt.*, vol. 3, no. 4, pp. 1184–1191, Oct. 2013.
[4] B. A. Veith-Wolf, S. Schäfer, R. Brendel, and J. Schmidt, "Reassessment of intrinsic lifetime limit in n-type crystalline silicon and implication on maximum solar cell efficiency," *Sol. Energy Mater. Sol. Cells*, vol. 186, pp. 194–199, 2018.
[5] R. Lang *et al.*, "MOVPE growth of GaAs with growth rates up to 280 μm/h," *J. Cryst. Growth*, vol. 537, 2020, Art. no. 125601.
[6] W. Metaferia *et al.*, "Gallium arsenide solar cells grown at rates exceeding 300 μm h-1 by hydride vapor phase epitaxy," *Nature Commun.*, vol. 10, no. 1, 2019, Art. no. 3361.
[7] N. Jain *et al.*, "III–V solar cells grown on unpolished and reusable spalled Ge substrates," *IEEE J. Photovolt.*, vol. 8, no. 5, pp. 1384–1389, Sep. 2018.
[8] S. Essig *et al.*, "Raising the one-sun conversion efficiency of III–V/Si solar cells to 32.8% for two junctions and 35.9% for three junctions," *Nature Energy.*, vol. 2, 2017, Art. no. 17144.
[9] R. Müller *et al.*, "Silicon-based monolithic triple-junction solar cells with conversion efficiency >34%," in *Proc. 37th Eur. Photovolt. Sol. Energy Conf. Exhib.*, 2020, pp. 574–578.
[10] D. Lackner *et al.*, "Two-terminal direct wafer-bonded GaInP/AlGaAs//Si triple-junction solar cell with AM1.5g efficiency of 34.1%," *Sol. RRL*, vol. 4, 2020, Art. no. 2000210.
[11] S.-T. Hwang *et al.*, "Bandgap grading and Al0.3Ga0.7As heterojunction emitter for highly efficient GaAs-based solar cells," *Sol. Energy Mater. Sol. Cells*, vol. 155, pp. 264–272, 2016. [Online]. Available: http://www.sciencedirect.com/science/article/pii/S0927024816301817
[12] P. R. Sharps *et al.*, "Development of 20% efficient GaInAsP solar cells," in *Proc. Conf. Rec. 23rd IEEE Photovolt. Specialists Conf.: Galt House Hotel*, Louisville, KY, USA, May/Oct. 1993, pp. 633–638.
[13] N. Jain *et al.*, "Development of lattice-matched 1.7 eV GaInAsP solar cells grown on GaAs by MOVPE," in *Proc. Conf. Rec. 43rd IEEE Photovolt. Specialists Conf.*, Portland, OR, USA, 2016, pp. 46–51.

[14] G. Létay and A. W. Bett, "EtaOpt—sA program for calculating limiting efficiency and optimum bandgap structure for multi-bandgap solar cells and TPV cells," in *Proc. 17th Eur. Photovolt. Sol. Energy Conf. Exhib.*, Munich, Germany, 2001, pp. 178–181.

[15] P. Schygulla, F. Heinz, D. Lackner, and F. Dimroth, "Subcell development for wafer-bonded III-V//Si tandem solar cells," in *Proc. IEEE 47th IEEE PVSC*, 2020, pp. 2716–2719.

[16] J. F. Geisz *et al.*, "Enhanced external radiative efficiency for 20.8% efficient single-junction GaInP solar cells," *Appl. Phys. Lett.*, vol. 103, no. 4, 2013, Art. no. 041118.

[17] I. Vurgaftman, J. R. Meyer, and L. R. Ram-Mohan, "Band parameters for III-V compound semiconductors and their alloys," *J. Appl. Phys.*, vol. 89, no. 11, pp. 5815–5875, 2001.

[18] P. T. Webster *et al.*, "Measurement of InAsSb bandgap energy and InAs/InAsSb band edge positions using spectroscopic ellipsometry and photoluminescence spectroscopy," *J. Appl. Phys.*, vol. 118, no. 24, 2015, Art. no. 245706.

[19] P. Würfel, *Physics of Solar Cells—From Principles to New Concepts*. Weinheim, Germany: Wiley-VCH, 2005.

[20] H. A. Zarem *et al.*, "Direct determination of the ambipolar diffusion length in GaAs/AlGaAs heterostructures by cathodoluminescence," *Appl. Phys. Lett.*, vol. 55, no. 16, pp. 1647–1649, 1989.

[21] R. Sinton and A. Cuevas, "A quasi-steady-state open-circuit voltage method for solar cell characterization," in *Proc. 16th Eur. Photovolt. Sol. Energy Conf.*, 2000, pp. 1152–1155s.

[22] A. P. Kirk and W. P. Kirk, "First principle analyses of direct bandgap solar cells with absorbing substrates versus mirrors," *J. Appl. Phys.*, vol. 114, no. 17, 2013, Art. no. 174507.

[23] pv-tools GmbH, *LOANA*. Accessed: Mar. 1, 2021. [Online]. Available: http://www.pv-tools.de/

[24] E. Centurioni, "Generalized matrix method for calculation of internal light energy flux in mixed coherent and incoherent multilayers," *Appl. Opt.*, vol. 44, no. 35, 2005, Art. no. 7532.

[25] P. Schygulla, P. Fuß-Kailuweit, O. Höhn, and F. Dimroth, "Determination of the complex refractive index of compound semiconductor alloys for optical device modelling," *J. Phys. D: Appl. Phys.*, vol. 53, no. 49, 2020, Art. no. 495104.

[26] S. Birner *et al.*, "Nextnano: General purpose 3-D simulations," *IEEE Trans. Electron. Devices*, vol. 54, no. 9, pp. 2137–2142, Sep. 2007.

[27] R. Lang, J. Schon, F. Dimroth, and D. Lackner, "Optimization of GaAs solar cell performance and growth efficiency at MOVPE growth rates of 100 μm/h," *IEEE J. Photovolt.*, vol. 8, no. 6, pp. 1596–1600, Nov. 2018.

[28] H. Kakinuma, M. Mohri, and M. Akiyama, "Characterization of oxygen and carbon in undoped AlGaAs grown by organometallic vapor-phase epitaxy," *Jpn. J. Appl. Phys.*, vol. 36, pp. 23–28, 1997.

[29] R. K. Ahrenkiel, "Minority-carrier lifetime and diffusion length in AlGaAs," in *Properties of Aluminium Gallium Arsenide*, vol. 7, S. Adachi, Ed., London, U.K.: IET, 1993, pp. 221–224.

[30] M. Niemeyer *et al.*, "Minority carrier diffusion length, lifetime and mobility in p-type GaAs and GaInAs," *J. Appl. Phys.*, vol. 122, no. 11, 2017, Art. no. 115702.

[31] P. M. Mooney, "Deep donor levels (DX centers) in III-V semiconductors," *J. Appl. Phys.*, vol. 67, no. 3, pp. R1–R26, 1990.

[32] S. Heckelmann, D. Lackner, and A. W. Bett, "Energy level of the Si-related DX-center in $(Al_yGa_{1-y})_{1-x}In_xAs$," *Appl. Phys. Lett.*, vol. 106, no. 10, 2015, Art. no. 102104.

[33] M. L. Timmons *et al.*, "Measurement of AlGaAs/AlGaAs interface recombination velocities using time-resolved photoluminescence," *Appl. Phys. Lett.*, vol. 56, no. 19, pp. 1850–1852, 1990.

[34] S. Adachi, *GaAs and Related Materials: Bulk Semiconducting and Superlattice Properties*. Singapore: World Scientific, 1994.